Physics in Collision - Zeuthen, Germany, June 26-28, 2003

QCD at e^+e^- Experiments

Klaus Hamacher
Fachbereich Physik, Bergische Univ., Gauß-Straße 20, 42097 Wuppertal

ABSTRACT

A summary of QCD results obtained at e^+e^- experiments in recent years is given. Emphasis is put on basic QCD tests and α_s measurements with event shapes.

1 Introduction

Experimental studies of strong interaction physics at e^+e^- machines aiming for basic tests of Quantum Chromodynamics, QCD, enfold the determination of the coupling and the quark masses, the parameters of the Lagrangian , the verification of the basic vertices of QCD, and tests of the loop corrections interrelated with asymptotic freedom and confinement. Moreover the experimentalists are faced with a wealth of strong interaction physics phenomena.

e^+e^- annihilation to hadrons provides the simplest strongly interacting initial state, a quark anti-quark pair. Actual measurements span from the Φ resonance at DaΦne to $\sqrt{s} \sim 209\,\mathrm{GeV}$ at LEP II. This talk reviews some basic measurements performed by e^+e^- experiments in recent years.

Results still come up from the measurements at the Z where the cross–section is large and background free precision measurements can be performed. At higher energy the measurements are complicated by frequent initial state photon radiation, leading to "Z return" events, and boson (W^+W^- and ZZ) pair production. Still the LEP data in combination with previous low energy results allow detailed tests of the energy evolution of hadronic properties.

Off resonance data from the B factories are important for studies of charm final states as, in this case, the charmed hadrons are not influenced by B hadron decay products. Moreover radiative Onia decays so far provide the only lucid source of purely gluonic final states.

2 Energy Dependence of the Hadronic Multiplicity

The dependence of the charged hadron multiplicity on the CMS energy up to the highest LEP II energies is shown in Fig. 4. The basic process governing the multiplicity increase is gluon Bremsstrahlung off the initial $q\bar{q}$ pair ($\propto C_F \cdot \alpha_s$; $C_F = 4/3$). The measurements are well described by parton shower (PS) fragmentation models, as well as by Modified Leading Log Approximation (MLLA) and 3NLO calculations [1]. The calculations intrinsically predict the number of final state gluons and quarks, the connection to the hadronic multiplicity being made by Local Parton Hadron Duality (LPHD) assuming the number of hadrons to be proportional to the number of partons. The proportionality factor is fitted to data, leaving only the energy increase predictable.

An important common aspect of all descriptions is the suppression of soft gluon emission due to gluon coherence. Impressive evidence for this phenomenon

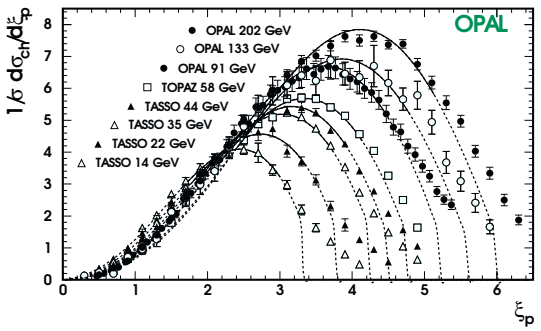

Figure 1: *CMS energy dependence of the spectra of charged hadrons [3] as function of* $\xi = -\ln x$*;* $x = 2E_h/E_{CM}$.

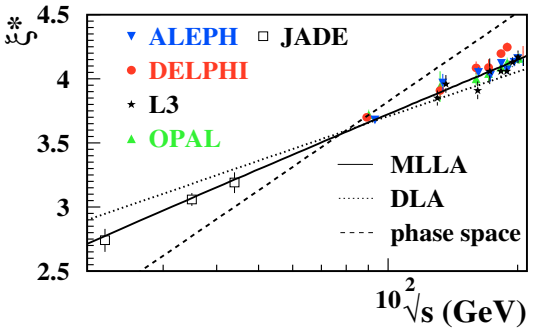

Figure 2: *CMS energy dependence of the maximum of the* ξ *distribution,* ξ^*.

comes from the "hump-backed" plateau shown in Fig. 1 depicting the suppression of low energy hadrons. The data over a wide energy range are compared to the MLLA "limiting spectrum" prediction. The increase of the maximum value, ξ^*, of these spectra is strongly reduced compared to phase space expectation (Fig. 2).

Independent insight on gluon coherence stems from the multiplicity difference, δ_{bl}, between light $l = uds$ and b quark events. In b events the collinear divergence of gluon radiation is regulated by the b mass. Radiation is suppressed within a "dead cone" of opening angle $\Theta \propto m_b/E$, i.e. Θ decreases towards high b energies. The corresponding increase in phase space for radiation and gluon coherence lead to the expectation of constant δ_{bl}. This expectation has been recently verified by LEP II measurements [2]. By contrast, incoherent radiation would lead to a strong decrease with energy: $\delta_{bl} \sim 2\langle N_B\rangle + N_{l\bar{l}}((1-\langle x_B\rangle)^2 s) - N_{q\bar{q}}(s)$, with $\langle x_B\rangle$ the average energy fraction and $\langle N_B\rangle$ the average decay multiplicity of B hadrons.

Analogously to the quark case the multiplicity in gluon jets is governed by gluon Bremsstrahlung off gluons ($\propto C_A\alpha_s$). Due to the higher colour factor $C_A = 3$, a multiplicity increase by the factor $C_A/C_F = 2.25$ is expected at high energy. Experimental results obtained mainly in e^+e^- 3 jet events were found in the range $1 \ldots 1.5$. The small ratio is now understood considering gluon coherence (leading to $p_\perp$ like scales), finite-energy/non-perturbative (n.p.) effects and biases due to jet selection.

Evidence for n.p. effects comes from the rapidity spectrum of hadrons in "leading" gluon jets recoiling with respect to a $b\bar{b}$ system of comparably small inter quark angle $\sim 90°$ [4]. For small rapidity, i.e. for particles produced first in the hadronisation, the production rate is about twice as high as for quark jets of corresponding energy. At high rapidity however, more hadrons are produced in quark jets. This is partly due to leading particle effects – quarks are "valence"

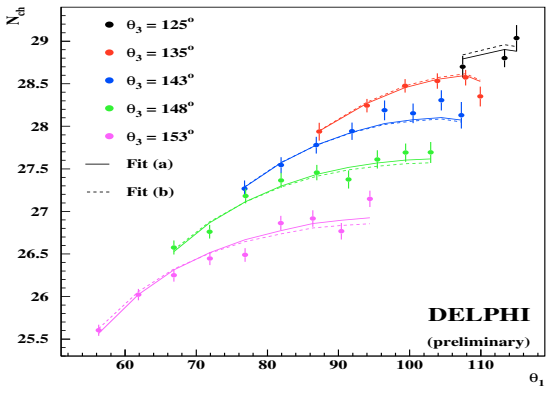

Figure 3: *Charged hadron multiplicity of three jet events as function of the inter jet angles.*

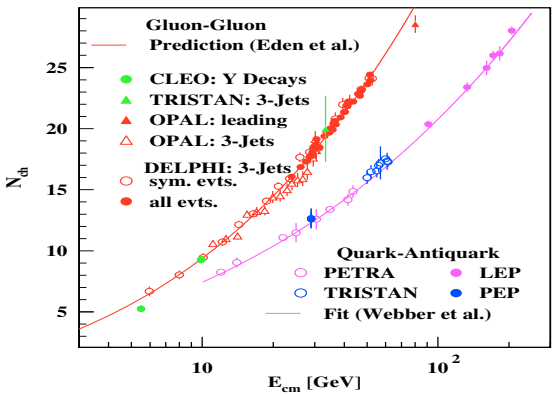

Figure 4: *Charged multiplicity for $q\bar{q}$ and gg colour singlet states as function of the CMS energy.*

particles of hadrons. Moreover, as Bremsstrahlung is less effective in quark jets, more energy remains available and allows high energy hadrons to be formed. The multiplicity of 3 jet events is predicted [5] as:

$$N_{q\bar{q}g} = N_{q\bar{q}}(s_{q\bar{q}}, y_{cut}) + \frac{1}{2} N_{gg}(p^2_{\perp g}) \quad , \tag{1}$$

where $N_{q\bar{q}}$ is the multiplicity observed in e^+e^- annihilation, N_{gg} is the multiplicity for a colour singlet gg pair. The choice of scales $s_{q\bar{q}}$ and $p^2_{\perp g}$ is ambiguous. It depends on the part of phase space assigned to the quark and gluon jets in a 3 jet event, respectively. The y_{cut} dependence enters solely due to a bias induced by the jet assignment. For a 3 jet event resolved at a selected y^0_{cut} it is prohibited to have further gluons emitted at higher $y^1_{cut} > y^0_{cut}$ as these would lead to $y^0_{cut} = y^1_{cut}$. Consequently a negative bias on the multiplicity is implied.

The energy slopes of the multiplicity of gluons and quarks are related by:

$$\left.\frac{dN_{gg}}{dL'}\right|_{L'=L+c_g-c_q} = \frac{C_A}{C_F}\left(1 - \frac{\alpha_0 c_r}{L}\right)\frac{d}{dL} N_{q\bar{q}}(L) \qquad L = \log\frac{s}{\Lambda^2} \qquad c_i = \text{const.} \tag{2}$$

The solution of this differential equation implies a const. of integration suited to absorb n.p. qg differences. The complete ansatz describes the observed multiplicity for 3 jet events of general (Fig. 3) and symmetric topology [6]. The energy scales are determined from the 3 jet topology and the three possible assignments of the gluon jet are considered by appropriate weighting with the 3 jet matrix element. Eq. (1) is easily solved for N_{gg}. The observed increase with energy is about twice that of the quark case (Fig. 4) and can be immediately recognized as due to the higher colour charge of the gluon. The quark curve is a MLLA fit to the data, the gluon curve is a

prediction deduced from the $q\bar{q}$ data using Eq. (2). The n.p. offset was fixed by the CLEO point at $\sqrt{s} \sim 10\,\text{GeV}$ measured from $\chi_B \to gg$ decays [7]. The prediction agrees with the 3 jet data from TRISTAN and LEP [6]. From symmetric 3 jet events DELPHI measured the colour factor ratio:

$$\frac{C_A}{C_F} = 2.221 \pm 0.032_{\text{stat.}} \pm 0.047_{\text{exp.}} \pm 0.058_{\text{hadr.}} \pm 0.075_{\text{theo.}} \tag{3}$$

3 Heavy Quark Fragmentation

Despite their complex decay patterns heavy hadrons can be reconstructed due to their long lifetime. Since heavy quarks are rarely produced in fragmentation it is possible to determine even the fragmentation function of primary B and D hadrons.

The expendable micro–vertex detectors of the LEP/SLC experiments allow inclusive B reconstruction with high purity and efficiency at a $\mathcal{O}(10\%)$ energy resolution. The new measurements of the b fragmentation function [8] (Fig. 5) agree with each other. Note however, that the data points are correlated due to the limited energy resolution and the unfolding applied in the analysis. The precise average of the scaled energy fraction $\langle x_B \rangle = 0.715 \pm 0.003$ of weakly decaying B's is slightly increased compared to previous e^+e^- results. This may be due to the inclusion of B baryons in the sample. The measurements now allow to distinguish between different fragmentation models. Consistency is only obtained with the Lund and the similar Bowler model while the data disagree with the widely used Peterson model. Very precise data on c fragmentation also became recently available [9]. The BELLE measurement is based on exclusively reconstructed D^{*+} mesons while CLEO also uses D^0 and D^+ decays. To avoid contamination from B decays at low x_D off resonance data ($\mathcal{L} \sim 3fb^{-1}$) are used. For $x_D > 0.5$, where B feed through is kinematically excluded, also the huge $\Upsilon(4S)$ data sets ($\mathcal{L} \sim 6 - 25fb^{-1}$) are used.

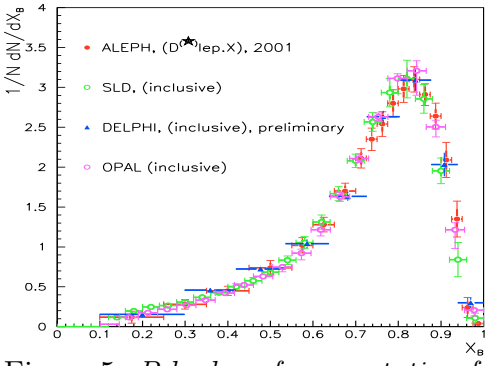

Figure 5: *B hadron fragmentation function as measured by* SLD *and* LEP.

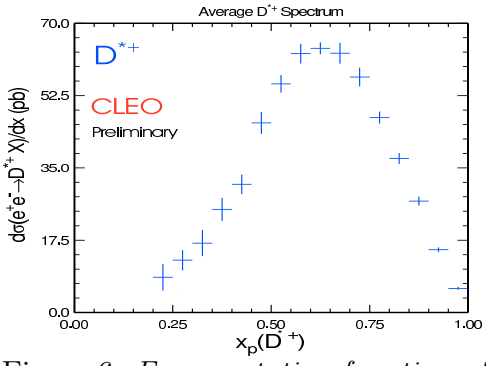

Figure 6: *Fragmentation function of* D^* *mesons as measured by* CLEO.

The momentum resolution is excellent due to the low CMS energy. The BELLE measurement gives $\langle x_p^{D*} \rangle = 0.612 \pm 0.003_{stat} \pm 0.004_{syst}$ and strongly favors the Bowler model. CLEO observes differences in the spectra of D^{*+}, D^0 and D^+, which are likely due to differing influence of D resonance decays. Such effects have to be considered when interpreting the precise results [9].

The application of the e^+e^- heavy quark results in the description of other processes requires a proper extraction of the n.p. fragmentation function. The e^+e^- analyzers now perform this extraction [10]. According to the QCD factorisation theorem the measured function is a convolution of a pert. piece, describing hard and soft gluon radiation, and the genuine n.p. fragmentation function. After Mellin transformation the convolution turns into a simple product of transformed contributions. This equation can be easily solved for the n.p. part and transformed back. The resulting n.p. B fragmentation function as evaluated from two LEP measurements agrees well [10] . It is strongly peaked around $x_b \sim 0.9$ showing that most of the b quark energy is conserved in the B hadron. This function can be directly applied in theoretical predictions provided similar assumptions (like renormalisation scheme and factorisation scale) are used in the application as in the e^+e^- pert. calculation.

The SLD experiment measured the double inclusive B fragmentation function [11]. This function depends on the energies of and the angle, Φ, between the B particles. The ratios G_{mn} of the double to the two corresponding single Mellin moments were determined. These ratios are advantageous for two reasons: The collinear singularity is canceled by the finite b mass and large log. terms $\propto \ln E_{cm}/m_b$ cancel to all orders [12]. The prediction for $G_{mn}(\Phi)$ agrees well with the measurement[11, 12]. As the n.p. fragmentation function enters twice in G_{mn} SLD interprets their measurement as a basic test of the QCD factorisation theorem. The theoretical work [12] suggests G_{mn} for a precise extraction of α_s.

4 Measuring $\mathbf{m_b(M_Z)}$

Besides the coupling the quark masses are the only free parameters of the QCD Lagrangian. The rôle of the masses is similar to that of the coupling. Besides the pole mass, M_q, therefore the renormalised mass, $m_q(Q)$, is defined, customarily in the $\overline{\rm MS}$ scheme. Quarks are bound inside hadrons, therefore their masses can be assessed only via dynamical relations. At high energy it is possible to determine the mass of the b quark from the reduction of gluon Bremsstrahlung in b compared to light quark events. This reduction is $\propto m_b^2/p_{\perp g}^2 \approx m_b^2/(s \cdot y_{cut})$. The $1/y_{cut}$ factor

increases the effect by one order of magnitude compared to the directly expected m_b^2/s dependence. Several coinciding predictions exist (see [13]).

The $m_b(M_Z)$ measurements performed by most of the LEP/SLC experiments [13] proceed as follows: Jet rates or event shapes are measured for b and light quark (or all) events. Heavy quark tagging is performed using impact parameter based techniques. Detector and hadronisation corrections partly cancel in the ratio R_3^{bl} of b and light distributions leading to controllable uncertainties despite the weak effect $\sim 3\%$ at $\sqrt{s} = M_Z$.

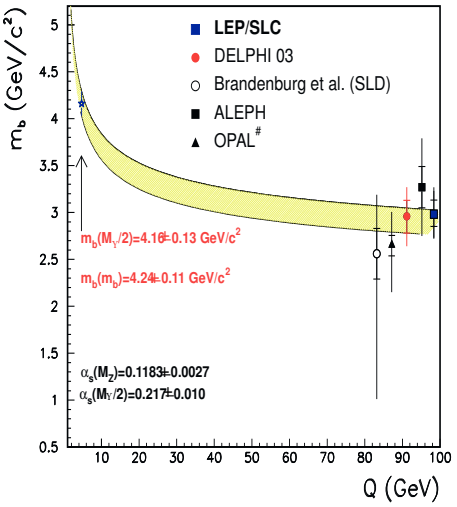

Figure 7: *E dependence of* $m_b^{\overline{MS}}$

Improved understanding of the hadronisation correction has been gained lately [14]. Apparent differences between models were traced to an imperfect prescription of the x_B distribution. The new DELPHI analysis avoids badly described regions henceforth leaving the associated uncertainty unimportant. A toy simulation connecting the different b quark masses and effects in PYTHIA with each other showes for the first time the expected stability of the hadronisation correction against parameter changes. However, the uncertainty of the b mass in the model, which could be identified with the pole mass, now appeared as important additional uncertainty.

The expected $\propto y_{cut}^{-1}$ dependence of R_3^{bl} is seen [13] and the data are consistent with the NLO expectation for $m_b(M_Z) \sim 3\,\mathrm{GeV}$. This small value already indicates the expected "running" of the mass seen in Fig. 7. Here the average $m_b(m_b)$ determined from bound states is compared to the $m_b(M_Z)$ results and their average:

$$m_b(M_Z)^{ADO/SLC} = 2.95 \pm 0.15_{stat} \pm 0.24_{hadc/theo} \quad . \tag{4}$$

For the averaging, theoretical and hadronisation uncertainties were taken fully correlated. The stat. error of OPAL determined from a correlated average has been scaled according to PDG rules with $\sqrt{\chi^2/N_{df}}$ of this average. Improved measurements of $m_b(m_b)$ from moments of the lepton spectra of B decays or using lattice calculations are expected [15]. The fall off of the mass with energy is given by the Renormalisation Group Equation:

$$\frac{\partial \ln m(Q^2)}{\partial \ln Q^2} = -\gamma_m(\alpha_s) \qquad \gamma_m \sim \quad , \tag{5}$$

where γ_m is the mass anomalous dimension, sensitive to loop corrections to the quark propagator. The succesful description of the b quark mass running implies a basic test of the quantum loop structure of QCD.

5 Four Jet Events and Colour Factors

In 4 jet events all basic QCD vertices except the suppressed quartic gluon vertex occur as building blocks already at tree level. At tree level the 4 jet cross–section can be decomposed into terms proportional to the colour factor products C_F^2, $C_F C_A$ and $C_F n_f T_F$. This possibility is due to the general helicity structure of the process and allows measurements of the colour factor ratios C_A/C_F and $n_f T_F/C_F$ from the 4 jet angular distributions. This is equivalent to a determination of the gauge group underlying the strong interaction. Recently NLO predictions for the cross–section became available (for references see [16]) improving the data description. At the cost of a leading order determination it is thus possible to determine directly the colour factors C_A and C_F, as well as α_s in combination with measurements of the 3 jet rate [16]. The current averages of the colour factors are:

$$C_F = 1.34 \pm 0.23 \qquad\qquad C_F = 2.97 \pm 0.5 \tag{6}$$

The results for the colour factor ratios are included in Fig. 14. A drawback of all measurements is the residual dependence on a necessary hadronisation correction. Here QCD is presumed uncared if MC models or QCD power corrections are used.

6 α_s from Event Shapes

The measurement of α_s with event shape observables probes the amount of gluon radiation in the hadronic final state $\propto C_F \cdot \alpha_s$. It is insensitive to the underlying electroweak physics. Event shape observables are required to be insensitive to soft and collinear gluon emission as well as to hadronisation effects. A typical observable is $t = 1 - Thrust$. In the following an arbitrary observable is denoted by y, where low values indicate small and large values ($y \sim 0.3$) imply hard gluon radiation.

The α_s measurement proceed as follows: The experimental distributions are determined and corrected for cuts, limited detector acceptance and resolution. At high energy Z return events and two boson production need special regard.

Two different types of predictions are available based on NLO α_s matrix element (ME) and Next to LLA (NLLA) calculations. The former applies to hard radiation, the latter to the two jet regime (small y) where multiple gluon emission

needs to be resummed. Both calculations can be matched in order to obtain a prediction valid for a wide region of phase space.

When comparing theory to data it is important to correct the influence of the n.p. hadronisation. The classical correction is given by the ratio of the y distribution on parton (that is just before hadrons are formed) to hadron level in a Monte Carlo model. Alternatively so called Power corrections (PC) are used.

6.1 α_s from NLO Matrix Elements

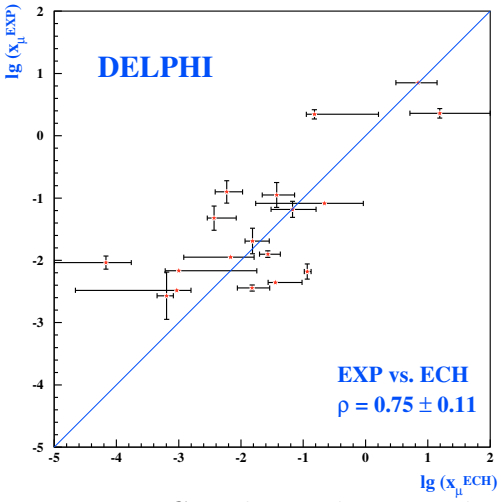

Figure 8: *Correlation between the experimentally optimised scale and the scale corresponding to the ECH scheme.*

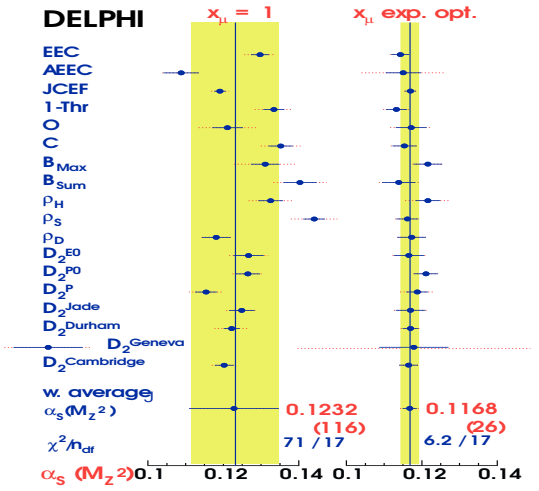

Figure 9: $\alpha_s(M_Z)$ *as determined from 18 observables from* DELPHI *data using* $\mathcal{O}(\alpha_s^2)$ *theory.*

The NLO prediction for the distribution of a 3 jet like observable is:

$$D(y) = \frac{1}{\sigma}\frac{d\sigma}{dy} = A(y)\bar{\alpha}_s(\mu) + [A(y)\beta_0 \ln x_\mu + B(y)]\bar{\alpha}_s^2(\mu) \qquad \bar{\alpha} = \frac{\alpha_s}{\pi} \tag{7}$$

where $A(y)$ and $B(y)$ are pert. calculated coefficients. For small y this prediction receives important higher order corrections $\propto \alpha_s \ln^2 y$. Uncalculated higher oder terms lead to the dependence on the unknown (observable dependent) renormalisation scale μ ($x_\mu = \mu^2/s$). The x_μ term changes the slope of $D(y)$, typically falling off exponentially at not too small y. Satisfactory agreement ($\chi^2/N_{df} \sim 1$) of the prediction is only obtained with optimised x_μ. Taking $x_\mu = 1$, that is the pure $\overline{\rm MS}$ prediction, will in general lead to a dependence of α_s on the chosen fit range. This fact was long known for small y but has also been verified at high y with the precise Z data [17]. In fact this behavior must persist at high y as a consequence of the normalisation of $D(y)$ to the total cross–section (see Eq. (7)).

The optimised scales for observables with large positive (negative) second order prediction tend to be small (high). Currently it is little understood why the experimentally optimised scales correlate with the theoretically motivated FAC/PMS/ECH scale choices (Fig. 8 [17]). The α_s results obtained using optimised scales only show a scatter of about 2%. For the $x_\mu = 1$ results, however, due to the aforementioned discrepancies the scatter is bigger $\sim 10\%$ for the same y intervals in the α_s fits. In this case an additional theory uncertainty is required in order to assure consistency of the α_s results obtained from different observables.

6.2 α_s from Matched $\mathcal{O}(\alpha_s^2) \oplus$ NLLA Predictions

The NLLA prediction has the general form:

$$R(y) = \int_0^y D(y)dy = \exp\left\{Lg_1(\alpha_s L) + g_2(\alpha_s L)\right\} \qquad L = -\ln y \quad . \tag{8}$$

The function $R(y)$, however, does not obey the phase space boundary conditions $R(y_{max}) = 1$, $\partial_y R(y_{max}) = 0$. This imperfection is corrected by the transformation:

$$L \longrightarrow L' = \frac{1}{p} \ln \left[\frac{1}{(x_L y)^p} - \frac{1}{(x_L y_{max})^p} + 1 \right] \quad , \tag{9}$$

where x_L and p are arbitrary parameters [18]. This transformation, though primarily modifying the prediction at high y also implies a % level shift in the α_s fit range.

In order to obtain a prediction valid over a large range of phase space the NLLA and NLO ME predictions for $x_\mu = 1$ are merged. Duplicated terms are subtracted by expanding the NLLA prediction in a power series in α_s. This subtraction is ambiguous as it can be performed for R or $\ln R$ (see Eq. (8)), respectively.

In Fig. 10 a comparison of the T distributions measured between the Z and 206 GeV and the matched prediction is shown. The data are well described over the full range of energy and T. Only for the precise Z data a slight difference in the slope is indicated. This difference is weaker for most other observables.

The LEP QCD Working Group attempts to combine the α_s measurements from the high energy (low statistics) LEP II measurements. The $\mathcal{O}(\alpha_s^2) \oplus$ NLLA prediction is use for the observables $1 - T$, M_h, C, B_t, B_w and y_3. The theory implementations and hadronisation corrections have been compared, the treatment of correlations and the theory uncertainty was discussed. It was seen that often badly described observables dominate in the combination and a downward bias in α_s was observed. This bias is due to the proportionality of the α_s theory uncertainty to α_s^3. To avoid these faults a novel definition of the theory uncertainty, the uncertainty

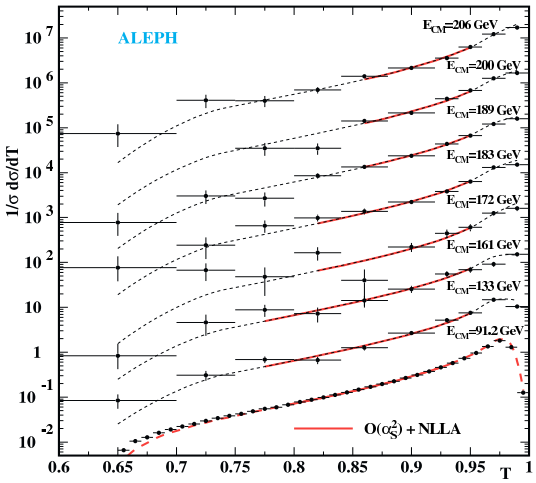

Figure 10: *Energy dependence of the Thrust distribution compared to the matched $\mathcal{O}(\alpha_s^2) \oplus$ NLLA prediction.*

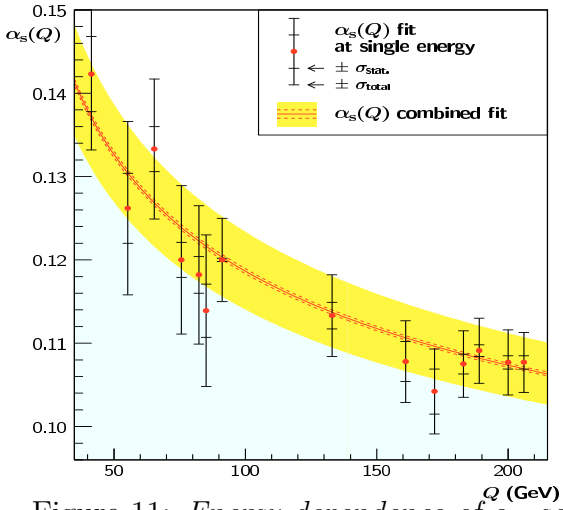

Figure 11: *Energy dependence of α_s as determined by the* LEP *QCD W.G. For data references see [19].*

band method, was introduced: the matched reference prediction with a fixed initial $\alpha_s(M_Z)$ was varied by changing the renormalisation scale ($1/2 < x_\mu < 2$), not applying or applying the NLLA phase space condition with $2/3 < x_L < 3/2$, $p = 1; 2$ and changing from $\ln R$ to R matching. The envelope of the variations defines the uncertainty band which in turn determines the uncertainty of the reference α_s. Using this fully correlated uncertainty as well as the experimental and hadronisation uncertainties the LEP average α_s is then calculated. The procedure is iterated until the result is stable. The results for $\alpha_s(M_Z)$ are [19]:

$$\text{LEP I}: \qquad 0.1200 \pm 0.0002_{stat} \pm 0.0008_{exp} \pm 0.0010_{had} \pm 0.0048_{th} \qquad (10)$$

$$\text{LEP II}: \qquad 0.1201 \pm 0.0005_{stat} \pm 0.0010_{exp} \pm 0.0007_{had} \pm 0.0045_{th} \qquad (11)$$

The observed energy dependence of α_s shown in Fig. 11 agrees well with the expectation. Despite the strongly different statistics the overall uncertainties of the LEP I and II results are comparable. This is due to the dominance of the theory uncertainty and a decrease in the hadronisation ($\propto 1/E$) and theory uncertainties ($\propto \alpha_s^3(E)$) with energy. The total uncertainty of the order 4% is confirmed by the scatter of the α_s results from the six individual observables studied.

6.3 Power Corrections (PC)

Assuming for the hadronisation process a longitudinal, "tube–like" phase space with fixed average transverse momentum, where only the rapidity range expands with increasing energy, E, it is easily shown that hadronisation corrections vanish $\propto 1/E$.

Also the replacement of the unknown analytical behavior of the strong coupling below an IR matching scale $\mu_I \sim 1 - 2\,\mathrm{GeV}$ by an effective average value $\alpha_0(\mu_I)$ leads to a inverse power law behavior [20]:

$$\mathcal{P} = \frac{4C_F}{\pi^2}\mathcal{M}\frac{\mu_I}{E_{\mathrm{cm}}}\left[\alpha_0(\mu_I) - \alpha_s(\mu) - \left(b_0 \cdot \log\frac{\mu^2}{\mu_I^2} + \frac{K}{2\pi} + 2b_0\right)\alpha_s^2(\mu)\right] \qquad (12)$$

For most observables the value y of the pert. calculation is just shifted by $+c_y\mathcal{P}$. Correspondingly its mean value $\langle y\rangle$ gains an additive correction. The constants c_y have been evaluated for NLLA resummable observables. The overall size of the PC, i.e. α_0, is determined from a fit to data. Within the uncertainty of the calculation ($\sim 20\%$) universal α_0 (and α_s) values are expected from the different observables.

The model scetched above is able to succesfully describe the data on distributions and means over a wide energy range [21, 22]. However, the obtained values of $\alpha_0 \sim 0.5$ are only consistent within the quoted uncertainty of the model. Specifically α_0 is smaller for mean values than for distributions. Due to the obvious correlation of α_0 and α_s (see Eq. (12)) this leads to a corresponding difference in $\alpha_s(M_Z)$. The JADE experiment for instance reports [22]:

$$\text{means:} \qquad \alpha_s(M_Z) = 0.1187 \pm 0.0014_{\mathrm{fit}} \pm 0.0001_{\mathrm{sys}}{}^{+0.0028}_{-0.0015\,\mathrm{th}} \qquad (13)$$

$$\text{distributions:} \qquad \alpha_s(M_Z) = 0.1126 \pm 0.0005_{\mathrm{fit}} \pm 0.0037_{\mathrm{sys}}{}^{+0.084}_{-0.060\,\mathrm{th}} \qquad (14)$$

This discrepancy persists even if hadron mass induced PC's are included[21].

6.4 Overview of α_s Results from LEP

Fig. 12 compares some important α_s results obtained from LEP data. All results are compatible with the current PDG average. The indirect measurements from the Z shape and R_τ are slightly above the average. The scatter of these partly highly correlated results obtained using NNLO theory confirms their error estimates.

The classical (3 & 4 jet) NLO direct measurements (with x_μ^{opt} and Monte Carlo hadronisation) agree well with the PDG average. The highly correlated result using matched theory is slightly higher also in comparison to the pure NLLA result. A shift towards higher α_s can be understood if the $\mathcal{O}(\alpha_s^2)|_{x_\mu=1}$ part of the matched prediction underestimates the slope of the data distribution. The results for means using PC's are slightly higher than the PDG average. Overall the scatter of the direct results confirms an error of $3-4\%$ of α_s typically assigned to the individual measurements. Improved predictions (like complete $\mathcal{O}(\alpha_s^3)$ ME's) are mandarory for any significant reduction of the uncertainty.

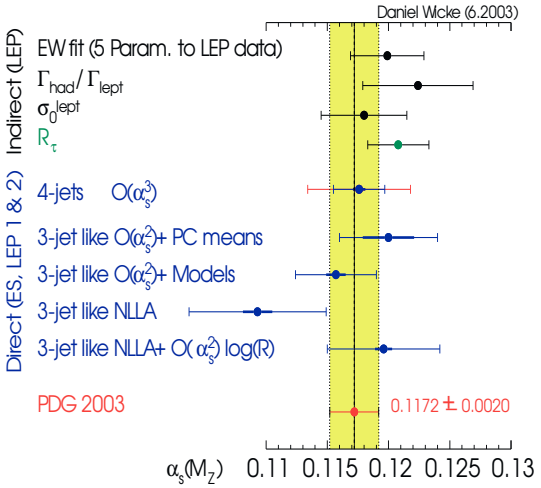

Figure 12: *Comparison of some important α_s results from* LEP.

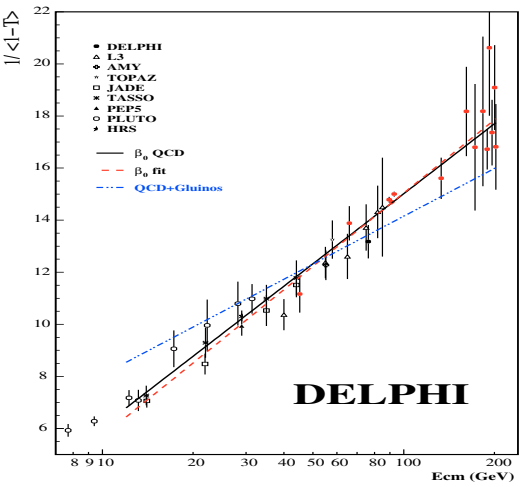

Figure 13: *Energy evolution of $\langle 1-T\rangle$. The slope determines the β function.*

6.5 The Running of α_s

The striking strong interaction physics phenomena of asymptotic freedom and confinement are intimately coupled to the energy evolution, the "running" of α_s. In QCD this is controlled by the Renormalisation Group Equation (RGE):

$$\frac{\partial \alpha_s}{\partial \ln Q^2} = -\alpha_s^2 \cdot \beta(\alpha_s) \qquad \frac{\partial \alpha_s^{-1}}{\partial \ln Q^2} = \beta(\alpha_s) = \frac{\beta_0}{4\pi}\left\{1 + \frac{\beta_1}{2\beta_0}\alpha_s + \rho_2\alpha_s^2 + \ldots\right\} \quad (15)$$

The β function describes the loop corrections to the gluon propagator, to leading order as:

$$\beta_0 = \frac{11}{3}C_A - \frac{2}{3}n_f \quad (16)$$

It is influenced by all strongly interacting particles. A measurement of the β function implies model independent limits on hypothetical strongly interacting particles. Such a measurement has recently been performed [21] based on the Renormalisation Group Invariant (or Improved) pert. theory (RGI p.t.). It applies to observables $R \propto \langle y\rangle/A$ depending on a single energy scale which are normalised such that their pert. expansion starts with α_s. RGI p.t. requires the observables to fulfil the RGE. This equation is solved as for α_s yielding an R dependent integration constant, Λ_R, which can be determined from a fit to the data. Λ_R is exactly related to $\Lambda^{QCD}_{\overline{MS}}$. RGI p.t. is numerically equivalent to the theory in the Effective Charge (ECH) scheme. E.g. RGI determines $\Lambda^{QCD}_{\overline{MS}}$ without freedom of renormalisation scheme choice. It is important to note that RGI p.t. implicitely resums UV divergencies. Power corrections can be included.

The RGI prediction has been fitted to the energy dependence of 7 event shape means [21]. The description of the data is equally good as with PC's though with less parameters. For RGI the power terms turned out to be compatible with zero ($\lesssim 2\%$ at the Z) and in contrary to the $\overline{MS}$+PC case all observables can be described with a single value of $\alpha_s = 0.1201 \pm 0.0020$. I.e. the energy dependence of mean values can be described at the 2% level without hadronisation correction and without renormalisation scale freedom. This implies that in the $\overline{MS}$ scheme power terms for mean values to a large part parameterise missing higher order terms. In fact it is even possible to predict the "n.p." terms using RGI [21].

To leading order the RGE (Eq. (15)) specifies a straight line when plotting the inverse of the observable vs. the logarithm of the energy, $\ln Q$. Thus, up to a small correction the slope of the data directly determines β_0. In order to optimally determine the β function data on $\langle 1-T \rangle$ has been chosen spanning the energy range 15 to 205 GeV(Fig. 13). A linear fit yields:

$$\frac{d\langle 1-T\rangle^{-1}}{d\ln Q^2} = 8.70 \pm 0.35 \quad , \tag{17}$$

consistent with the expected QCD value 8.32. This result model independently excludes supersymmetric gluinos up to masses of 30–40 GeV [21]. Assuming QCD β_0 or n_f can be alternatively determined:

$$\beta_0 = 7.83 \pm 0.32 \qquad\qquad n_f = 4.75 \pm 0.44 \quad . \tag{18}$$

This result is a clear measurement independent of assumptions about the β function unlike the case when using models in α_s determinations. It is superior to results from LEP ($\beta_0 = 7.67 \pm 1.63$) [19] or world data on α_s ($\beta_0 = 7.76 \pm 0.44$) [23].

7 Summary

Measurements performed at e^+e^- machines, especially those at and above the Z pole over the past decade provide a vast amount of hadonic physics results. For this talk the selected results appeared during the last few years.

Understanding of the dynamical behaviour of hadrons has been attained. Most important ingredience of the description here is the coherence of gluon radiation. Moreover it has recently been possible to verify the different coupling strengths of quark gluon and gluon gluon vertices directly from the hadrons created in three jet events.

The instrumentation of the experiments allowed detailed measurements of heavy quark production. Measurements of the heavy quark fragmentation function

will serve as an important input to hadron colliders. The measurement of the running of the b quark mass tests the loop structure of the b quark propagator.

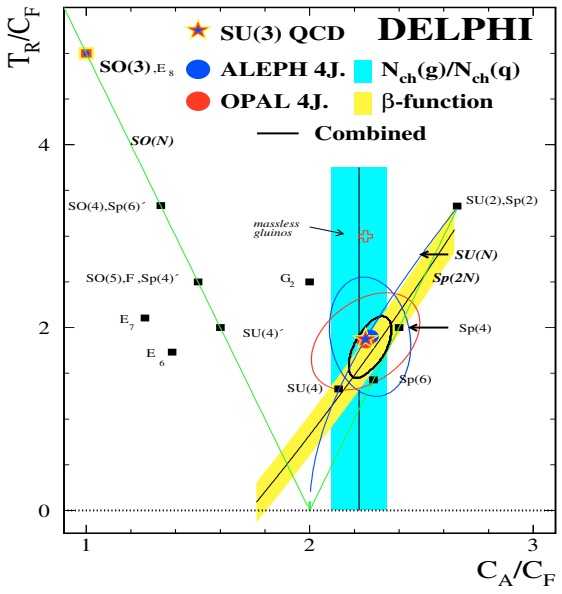

Figure 14: *Casimir factor ratios for several groups compared with constraints from various measurements.*

Several types of α_s measurements performed lead to a consistent result for the strong coupling, though with a still sizable uncertainty at the few % level. In most cases the uncertainty is dominated by the theory uncertainty. For a sizable reduction in α_s error improved predictions are required.

The measurements of the colour factors from 4 jet events, the multiplicity ratio obtained in gluon and quark jets and the quantum loops verified by the measurement of the β function strongly restrict the gauge group of strong interactions to $SU(3)$ / QCD (Fig. 14).

Acknowledgement

I thank P. Abreu, D. Duchesneau, G. Moneti, D. Muller, O. Passon, M. Siebel, H. Stenzel, R. Seuster and D. Wicke for providing input to this talk and O.P. and M.O. Dima for reading the manuscript.

References

1. H. Stenzel, talk at the EPS HEP Aachen (2003); I. M. Dremin & W. Gary, Phys. Lett. B **459** (1999) 341 and references therein.

2. P. Abreu *et al.*, Phys. Lett. B **479** (2000) 118, Erratum-ibid. B **492** (2000) 398; G. Abbiendi *et al.* Phys. Lett. B **550** (2002) 33 and P. Abreu, priv. comm.

3. G. Abbiendi *et al.* Eur. Phys. J. C **27** (2003) 467; H. Stenzel see [1] and D. Duchesneau, priv. comm.

4. G. Abbiendi *et al.* Eur. Phys. J. C **11** (1999) 217.

5. P. Edén, JHEP **9809** (1998) 015, P. Edén et al.,Eur. Phys. J. C **11** (1999) 345 and references therein.

6. K. Hamacher et al., CERN-OPEN-2000-134, P. Abreu *et al.* Phys. Lett. B **449** (1999) 383 and M. Siebel, DELPHI, priv. comm.; G. Abbiendi *et al.* Eur. Phys. J. C **23** (2002) 597; K. Nakabayashi *et al.* Phys. Lett. B **413** (1997) 447.

7. M. S. Alam *et al.* Phys. Rev. D **46** (1992) 4822; Phys. Rev. D **56** (1997) 17.

8. A. Heister *et al.* Phys. Lett. B **512** (2001) 30; K. Abe *et al.* Phys. Rev. Lett. **84** (2000) 4300; G. Abbiendi *et al.* arXiv:hep-ex/0210031; G. Barker et al., DELPHI 2002-069 CONF 603.

9. G. Moneti, CLEO priv. comm. and R. Seuster, talk at EPS HEP Aachen (2003).

10. E. Ben-Haim et al., arXiv:hep-ph/0302157.

11. K. Abe *et al.* SLAC-PUB-9289, contrib. to ICHEP, Amsterdam, 2002.

12. A. Brandenburg et al. arXiv:hep-ph/0304272.

13. P. Abreu *et al.* Phys. Lett. B **418** (1998) 430; A. Brandenburg et al., Phys. Lett. B **468** (1999) 168; R. Barate *et al.* Eur. Phys. J. C **18** (2000) 1; G. Abbiendi *et al.* Eur. Phys. J. C **21** (2001) 411, G. Rodrigo *et al.* arXiv:hep-ph/9905276.

14. M. J. Costa, thesis, Univ. Valencia 2003, P. Bambade et al., DELPHI 2003-05-03 Conf 435.

15. R. Sommer, these proceedings; M. Battaglia *et al.*, Phys. Lett. B **556** (2003) 41.

16. G. Abbiendi *et al.* Eur. Phys. J. C **20** (2001) 601 A. Heister *et al.* Eur. Phys. J. C **27** (2003) 1.

17. P. Abreu *et al.* Eur. Phys. J. C **14** (2000) 557.

18. The LEP QCD Working Group, R.W.L. Jones et al. in preparation.

19. The LEP QCD Working Group, DELPHI 2001-043 Phys 893, Aug. 8, 2003.

20. Y. L. Dokshitzer et al., JHEP **9907** (1999) 012 and references therein.

21. J. Abdallah *et al.* arXiv:hep-ex/0307048, R. Reinhard, thesis, Uni. Wuppertal, WUB-DIS 01-06, O. Passon, ibid. WUB-DIS 2002-06.

22. P. A. Movilla Fernandez et al., Eur. Phys. J. C **22** (2001) 1, also [21] and references therein.

23. S. Bethke, J. Phys. G **26**, R27 (2000).